Atmos. Meas. Tech., 5, 1953–1964, 2012
www.atmos-meas-tech.net/5/1953/2012/
doi:10.5194/amt-5-1953-2012

Atmospheric Measurement Techniques

Aerosol profiling with the Jenoptik ceilometer CHM15kx

M. Wiegner and A. Geiß

Ludwig-Maximilians-Universität, Meteorologisches Institut, Theresienstraße 37, 80333 Munich, Germany

Correspondence to: M. Wiegner (m.wiegner@lmu.de)

Received: 2 April 2012 – Published in Atmos. Meas. Tech. Discuss.: 8 May 2012
Revised: 5 July 2012 – Accepted: 13 July 2012 – Published: 13 August 2012

Abstract. Since a few years, the number of active remote sensing systems has been rapidly increasing as national weather services started to build up networks of ceilometers. As ceilometers can be considered as "simple" backscatter lidars, it is obvious to investigate to which extent they can provide quantitative aerosol information. In this context, the calibration of the ceilometer is the most crucial point: whereas previous studies primarily have relied on the comparisons with co-incident sun photometer measurements and the Rayleigh calibration, we provide an absolute calibration of the ceilometer. The advantage of this approach is that backscatter profiles can be derived during daytime and nighttime, and even in cases when the signal-to-noise ratio of signals from the free troposphere is very low. Moreover, the retrieval can easily be automated. In this paper, we consider the Jenoptik CHM15kx-ceilometer. We discuss the methodology and the achievable accuracy and present a set of examples to highlight the wide range of applications, and the limitations. The achievable temporal resolution is of the order of a few minutes; the relative error of the particle backscatter coefficient is less than 10 %. It is emphasized that the accuracy of extinction coefficients and – as a consequence – of the aerosol optical depth is limited due to the unknown lidar ratio. This is, however, an inherent problem of any backscatter lidar and not a special feature of the ceilometer.

1 Introduction

There is broad evidence that lidar is an excellent tool for aerosol remote sensing. Depending on the complexity of the systems with respect to number of wavelengths and the implementation of polarimetric channels, it is possible to derive a variety of properties to characterize aerosols. Backscatter lidars provide the derivation of geometrical properties (e.g., the detection of aerosol layers and their vertical extent), and advanced systems (high spectral resolution lidars or Raman lidars with polarimetric measurements) provide the assessment of optical properties, namely extensive properties such as the extinction coefficient as well as intensive properties such as the lidar ratio or depolarization ratio. This has been demonstrated in several field campaigns when lidars were key instruments to characterize specific aerosol types, including INDOEX (e.g., Müller et al., 2000), ACE-2 (e.g., Flamant et al., 2000; Ansmann et al., 2001), ACE-Asia (e.g., Shimizu et al., 2004), and AMMA (e.g., Heese and Wiegner, 2008). A recent example are the two SAMUM campaigns where Saharan dust was characterized near the source and at the beginning of its transport over the Atlantic Ocean (e.g., Groß et al., 2011; Tesche et al., 2011). During the last decade, lidar-related aerosol studies were extended towards attempts to derive microphysical properties (e.g., Böckmann, 2001; Kolgotin and Müller, 2008; Gasteiger et al., 2011).

Most of the current lidar activities are research oriented. This is in particular true when very complex systems are operated, but also when lidar networks are considered. Though the European aerosol research lidar network EARLINET (Bösenberg et al., 2003) – established in 2000, currently comprising 27 systems, and probably the most mature network worldwide – provides measurements on a regular schedule, it is far from being a monitoring network. EARLINET is focused on improvements of the hardware, the elaboration of robust data evaluation schemes including a complete error analysis and a strict quality control. Following this approach, it aims to ultimately establish a European aerosol climatology.

The benefit of these state-of-the-art lidar systems is undoubted; however, unattended and continuous operation of advanced lidar systems is still an exceptional case. As a consequence, the use of ceilometers as a sort of secondary

network is fostered. Ceilometers are simple one-wavelength backscatter lidars with low pulse energy and high pulse repetition frequencies. Recently, several weather services set up ceilometer networks, e.g., the German Weather Service (DWD) installed more than 50 systems in Germany. Ceilometers were originally designed to determine cloud base heights. Consequently, most studies are focused on the intercomparison of ceilometers of different manufacturers, and their ability to detect cloud layers (e.g., Martucci et al., 2010) compared to other remote sensing techniques (e.g., McKendry et al., 2009). Furthermore, the assessment of the boundary layer height was investigated (e.g., Emeis et al., 2004; Wiegner et al., 2006; Münkel et al., 2007; Haeffelin et al., 2011).

With the improvement of the ceilometer hardware, it became clear that there might be a certain potential for aerosol remote sensing. To be of benefit for aerosol research, it is desired to derive the aerosol extinction coefficient α_p as a function of height, or at least the backscatter coefficient β_p. It is obvious that the derivation of α_p suffers from the inherent problem of any backscatter lidar: as the lidar ratio S_p (defined as the ratio of the particle extinction and backscatter coefficients, α_p/β_p) is unknown, the retrieval of α_p is strongly influenced by the accuracy of the estimated lidar ratio. The accuracy of the retrieval of β_p normally is less sensitive to erroneous estimates of S_p, in particular at wavelengths in the near infrared. The calibration of lidar signals by means of an aerosol-free atmospheric layer – the so-called Rayleigh calibration – is not an issue for advanced lidar systems, but could raise serious problems in case of ceilometers. The reason is the low pulse energy of the laser resulting in a (very) low signal-to-noise ratio from layers in the free troposphere where aerosol-free conditions are expected. This is in particular true for daytime measurements.

One approach to evaluate ceilometer measurements is based on the combination with co-located and coincident sun photometer measurements (e.g., Takamura et al., 1994; Sicard et al., 2006; Heese et al., 2010). This approach relies on the photometer-derived aerosol optical depth, i.e., the integral of α_p over the atmospheric column, as a constraint for the inversion of the ceilometer signals. The underlying concept is to change the lidar ratio until there is agreement between the integral over α_p and τ_p. However, there are a number of problems associated with this approach: as sun photometer measurements are only available during daytime and under conditions of low cloudiness, the range of application is limited. Unfortunately, during nighttime, when the ceilometer is in principle better suited for aerosol remote sensing due to the missing background radiation, this methodology cannot be applied. The extrapolation of the optical depths from the previous or following day might be possible under stable conditions but will introduce additional uncertainties in any case. As the determination of aerosol optical depth at large solar zenith angles (sunset, sunrise) could be critical due to incorrect cloud clearing, the extrapolation to nighttime is further complicated. Another problem of the combined evaluation of ceilometer and sun photometer measurements is based on the region of incomplete overlap z_{ovl} of the ceilometer (Stachlewska et al., 2010). The larger z_{ovl} is, the more critical becomes the usage of τ_p to estimate the lidar ratio for the ceilometer inversion. This problem is insofar quite serious, as under typical conditions most of the particles are concentrated in the lowermost atmospheric layers. If this layer is below z_{ovl} and no reliable overlap correction is available, the adjustment of S_p by comparing optical depths is not possible.

For these reasons, we follow an approach briefly outlined by Wiegner (2010). It is based on the absolute calibration of the ceilometer and provides a more robust method to provide quantitative aerosol profiles. The methodology including a discussion of its accuracy is outlined in Sect. 2. In this paper, we use data of a Jenoptik ceilometer CHM15kx as explained in the following section. Next, the two-step calibration of the ceilometer is described in detail. To demonstrate the potential of the ceilometer with respect to aerosol profiling, we provide a few examples when the method is applied to measurements in Munich (Sect. 5). A brief summary concludes the paper.

2 Theoretical concept

The derivation of β_p (or α_p) in case of backscatter lidars is provided by the Klett or Fernald algorithm (Klett, 1981; Fernald, 1984). A general description of the concept can already be found in Fernald et al. (1972): in brief, α_p is expressed in terms of the transmission T_p and then inserted into the lidar equation. Then, a linear differential equation for T_p^2 is obtained. The solution requires an estimate of the lidar ratio S_p, whereas the lidar constant C_{L} is normally substituted by a boundary value $\beta_p(z_{\mathrm{ref}})$. The lidar constant comprises system parameters describing among others the efficiency of the detection unit and the energy of the laser pulse. Applying the so-called Rayleigh calibration, a height z_{ref} in the upper troposphere is selected that can be assumed to be free of aerosols. Thus, the aerosol backscatter coefficient is set to $\beta_p(z_{\mathrm{ref}}) = 0$ and can be used to calibrate the signals.

This solution can be expressed in an equivalent form that includes the lidar constant C_{L}, i.e, C_{L} is not replaced by a reference value. Then, β_p can be derived from the lidar signal $P(z)$ according to

$$\beta_p(z) = \frac{Z(z)}{S_p(z)\, N(z)} - \beta_{\mathrm{m}}(z) \tag{1}$$

with

$$Z(z) = S_p(z)\, z^2\, P(z) \exp\left\{-2 \int_0^z [S_p\, \beta_{\mathrm{m}} - \alpha_{\mathrm{m}}] \mathrm{d}z'\right\} \tag{2}$$

and

$$N(z) = C_{\mathrm{L}} - 2\int_0^z Z(z')\,\mathrm{d}z'. \quad (3)$$

Under realistic conditions, the functions Z and N are not calculated starting at the surface ($z = 0$, "integration in forward direction") but from the range of complete overlap z_{ovl}. This is justified if z_{ovl} is small and a wavelength in the near infrared is used, i.e., α and β are small. Both conditions are fulfilled in the case of the CHM15kx (see next section for details) and thus

$$\exp\left\{-2\int_0^{z_{\mathrm{ovl}}}[S_p\beta_{\mathrm{m}} - \alpha_{\mathrm{m}}]\mathrm{d}z'\right\} \approx 1 \quad (4)$$

and

$$\exp\left\{-2\int_0^{z_{\mathrm{ovl}}}\alpha(z')\mathrm{d}z'\right\} \approx 1. \quad (5)$$

Thus, the lower limits of the integrals in $Z(z)$ and $N(z)$ can be replaced by z_{ovl}. Note that, though there is a minus sign in the denominator, solution (see Eq. 1) does not become mathematically unstable due to the low optical depths in the near infrared ($C_{\mathrm{L}} \gg 2\int Z\mathrm{d}z$). The backscatter and extinction coefficients of the air molecules, β_{m} and α_{m}, can readily be calculated from the air density known from radiosonde ascents. Both variables are assumed to be known whenever lidar signals are evaluated.

It can be concluded that, when the lidar constant is known (frequently referred to as absolute calibration), the derivation of the backscatter coefficient profiles only requires an estimate of the lidar ratio. Whereas the conventional method based on the Rayleigh calibration is only applicable for systems that provide sufficient signal-to-noise ratios in the free troposphere, this alternative inversion is valid for any absolutely calibrated lidar or ceilometer with equal performance.

3 Ceilometer and data

In this paper, we use data of the Jenoptik ceilometer CHM15kx. The main specifications relevant for this study are briefly summarized. The system emits laser pulses at 1064 nm (Nd:YAG-laser, class M1) with a typical pulse energy of 8 µJ and a pulse repetition frequency of about 6500 Hz. The beam divergence is 0.33 mrad; the field of view is 1.8 mrad. In contrast to the Jenoptik ceilometer CHM15k, the optical axes of the laser and the telescope are tilted by 0.46 mrad. As a consequence, the height of complete overlap is very low with $z_{\mathrm{ovl}} \approx 150$ m according to own measurements and information provided by S. Frey (personal communication, 2012). The backscattered photons are measured by an APD in photon counting mode.

The CHM15kx of the Meteorological Institute (48.148° N, 11.573° E, altitude 539 m) of the Ludwig-Maximilians-Universität (LMU) in Munich, Germany, has been operated continuously since 16 June 2009. The data are stored with a temporal resolution of 30 s and a spatial resolution of 15 m. The maximum height of the signals is 15.36 km equivalent to 1024 range bins. The data are stored in NetCDF-format.

The sensitivity of the ceilometer changes automatically with the background radiation: during daytime and in case of low, bright clouds in the line of sight, the sensitivity is reduced. This is realized by reducing the high voltage supply of the APD. These modifications can be tracked from the data files: the difference between the actual and the breakdown voltage of the APD is stored in the NetCDF-files (parameter *NN1*, given in 0.1 Volt), henceforward referred to as Δ. The background signal is monitored by means of the "daylight_correction_factor" in the data file; here it is denoted as B for the sake of brevity. For our ceilometer, Δ ranges between 120 and 155. Whenever B exceeds 0.3, Δ is increased by 5. In some cases, more than one of these changes are made with in a few minutes, resulting in an effective increase of Δ of, for example, 10 or 15. Then, the system is adjusted to the new background and the detector-settings may be stable for hours again. An analogue procedure is effective when the background radiation decreases, e.g., after sunset or if highly reflecting clouds disappear from the line of sight. In these cases, Δ is decreased by 5 as soon as B is lower than 0.001. From our investigations, we found that about 85 % of all changes of Δ are not larger than ± 10.

The backscatter and extinction coefficients β_{m} and α_{m}, required to determine the optical properties of the particles (see Eq. 1), are calculated from pressure and temperature profiles of radiosonde ascents in Oberschleißheim, which is 10 km north of the ceilometer site.

4 Calibration of the ceilometer

The assessment of the lidar constant C_{L} in the case of the CHM15kx is complicated as the sensitivity of the detection unit changes under different meteorological conditions. Thus, the absolute calibration is carried out in two steps. One step provides the absolute calibration for a certain Δ. This is done in only 14 cases, because very strict requirements with respect to the independent data sets and the meteorological conditions must be fulfilled. Note that we have almost 1000 days of ceilometer observations (June 2009 until January 2012). The second step concerns the determination of the relative change of the lidar constant as a function of Δ. This part is performed in almost 250 cases, because this procedure only relies on the ceilometer data alone, and the meteorological requirements are met more easily. The combination of both parts provides the absolute calibration of all ceilometer measurements.

4.1 Relative calibration

A typical example of one day of measurements with several changes of the sensitivity of the system can be seen in Fig. 1. Shown is the time-height cross section of the range-corrected signal (Pz^2) (logarithmic scale, color coded in arbitrary units) of 22 April 2010; the vertical axis is the height above ground. The colors between light blue and red illustrate the high aerosol abundance in the boundary layer below 2 km; deep blue areas indicate low aerosol load and aerosol-free regions. Cloudiness is low throughout the day as can be seen from the few white areas. Changes of the sensitivity are clearly visible from the distinct changes of the colors: at 06:57 UTC when Δ changes from 135 to 150, at 08:28 UTC when Δ changes from 150 to 155, at 18:24 UTC (from 155 to 150) and at 19:27 UTC (from 150 to 145). With each modification, a change of C_L is associated. The changes at 01:00 UTC and at 13:30 UTC are discussed separately (see Sect. 4.3).

The relative change of C_L as a function of Δ is determined first. The decrease or increase of C_L during the change of the high voltage difference from Δ_i to Δ_j (corresponding to times t_i and t_j, respectively) can directly be determined from the ratio of the corresponding signals. If the aerosol distribution is constant during this time, all "atmospheric" terms ($\beta = \beta_\mathrm{m} + \beta_p$, and the transmission) in the lidar equation

$$P(t_i)\,z^2 = C_\mathrm{L}(t_i)\;\beta(z)\;\exp\left\{-2\int_0^z \alpha(z')\mathrm{d}z'\right\} \tag{6}$$

cancel out and a very simple relation for the conversion factor η_x remains:

$$\eta_x = \frac{C_\mathrm{L}(\Delta_j)}{C_\mathrm{L}(\Delta_i)} = \frac{P(t_j,z)}{P(t_i,z)} = \frac{P(t_j,z)\,z^2}{P(t_i,z)\,z^2}. \tag{7}$$

The conversion factors η_x are expressed in terms of the difference of Δ at t_j and t_i, which means η_{-5} stands for a decrease of Δ by 5 ($x = \Delta(t_j) - \Delta(t_i) = -5$, e.g., from 155 to 150), whereas η_5 describes an increase of Δ by 5.

The factors η_{-5} and η_5 are determined when the aerosol distribution is stable in the mixing layer, in particular below height z that is used in Eq. (7). Typically, z is selected in a height below 1000 m where the aerosol backscatter is strong enough that the signal is virtually unaffected by noise.

One example of the determination of the conversion factor η_{-5} is shown in Fig. 2. The range-corrected signals at $z = 585$ m are displayed from 19:00 UTC till 20:00 UTC (22 April 2010), and the temporal resolution is 30 s. At 19:27 UTC, Δ changes from 150 to 145 (cf. Fig. 1). To calculate η_{-5}, we consider a temporal average over 10 min before ($P(t_i)\,z^2$) and after ($P(t_j)\,z^2$) the change as indicated in the figure. Longer temporal averages seem to be neither necessary nor adequate as the signal slowly decreases due to a changing aerosol distribution. The accuracy of η_{-5} depends on the accuracy of the averages of the involved range-corrected signals and is estimated from a set of calculations with different temporal averages. In this case, we find a relative error of η_{-5} of 3.5 %. This number is typical. Note that we consider only cases when the atmosphere is stable in time. Thus, it can be expected that the associated errors of the conversion factors are small.

Following this procedure, conversion factors η_{-5} are determined for 111 cases. It is found that the conversion factor is virtually independent of Δ. In other words, a change of Δ from 150 to 145 and a change from 145 to 140 have the same effect on the signal strength. As can be seen in Table 1, $\eta_{-5} = 1.247$ on average, with an error of 0.033. The error is calculated from the individual errors of each of the 111 cases.

We also consider cases when the background radiation increases and consequently Δ increases. Analog to the previous paragraph, we calculate η_5 for any Δ. From a total of 23 cases, we find as an average $\eta_5 = 0.830$ with an error of 0.033. As an increase of Δ and a subsequent decrease of the same magnitude (or vice versa) should result in an unchanged sensitivity of the detection unit, it can be expected that $\eta_x = (\eta_{-x})^{-1}$ is valid. To make clear the good agreement between both values, we have included the inverse of η_5 in Table 1.

As already mentioned, also larger changes of Δ, as a rapid sequence of two or three steps, occur. From these cases, we calculate $\eta_{-10} = 1.540$ (63 cases) and $\eta_{-15} = 1.948$ (30 cases). It is expected that a decrease of Δ by 10 is equivalent to two subsequent decreases by 5 each, i.e., $\eta_{-10} = (\eta_{-5})^2$. For the same reasons, $\eta_{-15} = (\eta_{-5})^3$ should hold. Thus, we include the square root of η_{-10} and the cubic root of η_{-15} in Table 1. It can be seen that the results are in close agreement with the direct determination of η_{-5}. The corresponding conversion factors when Δ increases by multiples of 5 are determined in the same way.

From the good agreement of all cases when normalized to an Δ-decrease of 5, we define an "overall" conversion factor η according to

$$\eta = (\eta_x)^{-1/n} \tag{8}$$

with

$$x = (\Delta_j - \Delta_i) \qquad \text{and} \qquad n = \frac{(\Delta_j - \Delta_i)}{5}. \tag{9}$$

The exponent n ranges from $-3 \le n \le 3$, as x ranges from -15 to 15 in steps of 5. From Table 1, we find $\eta = 1.238 \pm 0.037$. From Eq. (8), it is clear that the knowledge of η is sufficient to account for any change of the sensitivity of the ceilometer: if $C_\mathrm{L}(\Delta_i)$ is known, we get $C_\mathrm{L}(\Delta_j)$ according to

$$C_\mathrm{L}(\Delta_j) = C_\mathrm{L}(\Delta_i)\eta^{-n}. \tag{10}$$

Equation (10) shows that $C_\mathrm{L}(\Delta_j) < C_\mathrm{L}(\Delta_i)$, if $\Delta_j > \Delta_i$.

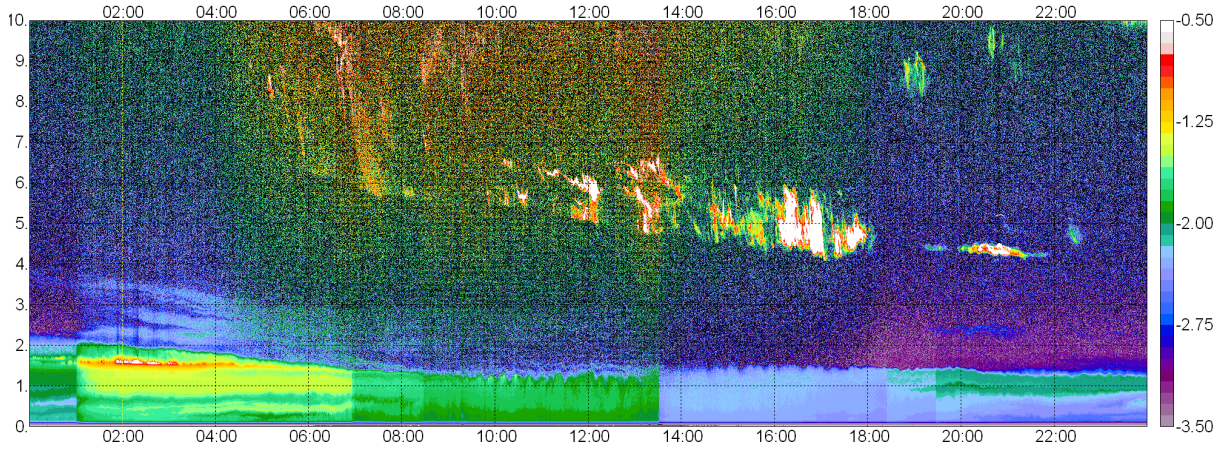

Fig. 1. Time height cross section of range-corrected signal (in logarithmic scale, a.u.) at 1064 nm from ceilometer CHM15kx in Munich, 22 April 2010. Changes in the sensitivity are obvious at 01:00 UTC, 06:57 UTC, 08:28 UTC, 13:30 UTC, 18:24 UTC, and 19:27 UTC.

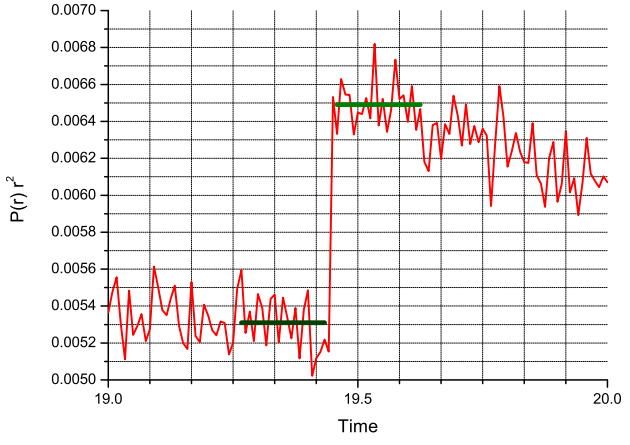

Fig. 2. Range-corrected signals at $z = 585$ m from 19:00 UTC to 20:00 UTC (22 April 2010) in intervals of 30 s. At 19:27 UTC, Δ changes from 150 to 145.

4.2 Absolute calibration

Measurements are considered suitable for the absolute calibration of the ceilometer when two conditions are fulfilled. The first condition is that the background radiation is low and Rayleigh calibration is possible for 60 to 120 min averages of the signals. Shorter time periods have been found to be unrealistic (Wiegner, 2010). The second condition is that the aerosol optical depth is derived independently from AERONET measurements (Holben et al., 1998) and can be used to constrain the lidar ratio of the Klett algorithm. This strategy is not a contradiction to the above-mentioned concerns about this approach: in our case the ceilometer's range of full overlap is very low so that the error of the "missing" optical depth is negligible. To illustrate this, we assume a typical $\alpha_p = 0.05\,\mathrm{km}^{-1}$ at $z = 150$ m. If we assume a constant α_p down to the ground, the optical depth of this "missing" layer is $\tau_{p,\mathrm{ovl}} = 0.0075$. Even a very large relative error of 50 % of α_p would result in an over- or underestimate of the optical depth of less than 0.004. Furthermore, we apply this method only when the time difference between the ceilometer measurement and the AERONET retrieval is below two to three hours, and when there are no indications that the aerosol distribution has undergone changes during that time period. For these reasons, we primarily choose cloud-free time periods close to sunset or sunrise.

Table 1. Conversion factors η as defined in Eq. (8) (see text for details).

	Average	Error	# cases
η_{-5}	1.247	0.033	111
$(\eta_{-10})^{1/2}$	1.241	0.031	63
$(\eta_{-15})^{1/3}$	1.249	0.023	30
$(\eta_{5})^{-1}$	1.205	0.048	23
$(\eta_{10})^{-1/2}$	1.186	0.024	10
$(\eta_{15})^{-1/3}$	1.184	0.016	7

If the aerosol extinction coefficient profile α_p is retrieved from the Klett algorithm, the lidar constant can directly be determined from the lidar equation (see Eq. 6 and discussion in Sect. 2):

$$C_\mathrm{L} = P\,z^2\,\beta(z)^{-1} \exp\left\{2\int_{z_\mathrm{ovl}}^{z} \alpha(z')\mathrm{d}z'\right\}. \quad (11)$$

For the assessment of the errors of C_L, we consider two main contributions: the error due to the uncertainty of τ_p as derived from the Cimel radiometer, and the error of the Rayleigh calibration. The uncertainty of τ_p based on a single measurement is typically 0.015 depending on the calibration

and the maintenance of the radiometer. Taking into account that we only select meteorological conditions when the aerosol stratification is stable, and that we average over one to two hours, the resulting error is certainly smaller. We estimate it from the variability of individual Cimel measurements during the calibration period; in all cases it is smaller than 0.006. Errors due to the different spatial sampling of the ceilometer (observing the vertical atmospheric column) and the radiometer (observing a slant path in the direction of the sun) are impossible to be quantified and assumed to be negligible. With respect to the Klett-algorithm, we assume that in the Rayleigh calibration range the scattering ratio $R = 1+\beta_p/\beta_m$ is not larger than 1.1. This uncertainty has a larger influence on the retrieved C_L than the uncertainty of τ_p. Due to these error sources, we get a range of possible solutions of C_L. This range can be described by $C_L \pm \Delta C_L$, where C_L is the mean of the maximum and minimum, and ΔC_L is defined as half of the difference of the maximum and the minimum; ΔC_L is considered as a systematic error.

As a result of the strict requirements, we get 14 cases suitable to calculate the lidar constant of the ceilometer. These cases include different values of Δ; the most frequent setting is $\Delta = 140$. According to the discussion in Sect. 4.1, the ratio of lidar constants should fulfill Eq. (10). Therefore, they can serve as an independent check of the validity of the calibration factor η. Finally, it is obvious from Eq. (10) that it is sufficient for the absolute calibration to define a reference value of the lidar constant C_L^* for one specific Δ_{ref}. We select $\Delta_{ref} = 140$.

An example of this procedure is given in Fig. 3. Shown is the range-corrected signal of the ceilometer (left panel) from 12 October 2010, averaged over two hours from 15:00 UTC till 17:00 UTC, and $\Delta = 140$. Within the boundary layer, it is smoothed over 105 m (7 range bins); in the free troposphere, a running mean over 31 range bins is applied. The hypothetical signal of the Rayleigh atmosphere is plotted to demonstrate the good agreement of the slopes of the signals in a height range around 4 km. The Klett inversion algorithm is applied to derive $\alpha_p(z)$, assuming a height-independent lidar ratio. The lidar ratio follows from the condition that the integrated aerosol extinction coefficient from the ceilometer data and the aerosol optical depth from the Cimel measurements (12 October 2010, 13:00–15:00 UTC) must agree. In this case, we find $S_p = 48 \pm 9$ sr, and a lidar constant of $C_L = 17.68 \pm 1.20$ km^3 sr (with P being dimensionless).

In Fig. 4 the lidar constants C_L^* as determined from the 14 cases with different Δ are shown; case no. 9 refers to the example discussed above. The conversion from the individual Δ-value to Δ_{ref} is applied according to Eq. (10), and the involved errors are considered. The good agreement of the lidar constants confirms the η-value derived in the previous section. The reference lidar constant is finally determined as the average over all cases and found to be $C_L^* = 17.39 \pm 0.67$ km^3 sr (corresponding to 3.9 %).

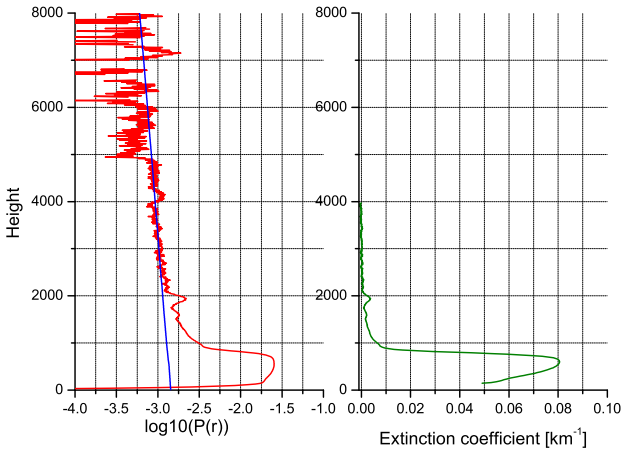

Fig. 3. Left panel: range-corrected signal of the ceilometer (red line) of 12 October 2010 at 16:00 UTC (two hours average) and the calculated signal for a Rayleigh atmosphere (blue line). Right panel: aerosol extinction coefficient α_p as retrieved from ceilometer measurements with a lidar ratio $S_p = 48$ sr. The lidar ratio is adjusted that the optical depth τ_p matches the quasi co-incident Cimel measurements (14:00 UTC, two hours average).

It is worthwhile to briefly discuss the lidar ratios that are found from the calibration (Fig. 5). The black squares mark the S_p that correspond to each of the 14 lidar constants. They range from 24 sr to 68 sr with an average of 43 sr. The uncertainty ranges of S_p are consistent with the uncertainty of the corresponding lidar constants (see Fig. 4). It seems that during summer and fall the lidar ratios are significantly lower compared to the other two seasons. It will be interesting whether an annual cycle can be confirmed by more and independent measurements. It should be stressed that Fig. 5 may not be misunderstood as a representative sample of a lidar ratio climatology over Munich; it is rather meant as a demonstration that no unrealistic lidar ratios are found when we calculate the lidar constant. Note that no lidar ratios derived from Raman lidar measurements in Munich in the framework of EARLINET are available for comparison, as they only concern 355 nm and 532 nm. With the limited data set currently available, we use $S_p = 43$ sr for all retrievals discussed later.

4.3 Special cases

When cumulus clouds develop at the top of the boundary layer and solar illumination is high, the background radiation could be quite strong. This situation is associated with a sudden rise of B and the exceedance of the threshold $B = 0.5$. From the point of aerosol remote sensing with a ceilometer, these situations are less relevant – for the investigation of cloud-aerosol interactions, one would rather rely on multi-wavelength lidar observations. Nevertheless, very high background conditions can also happen when the derivation of

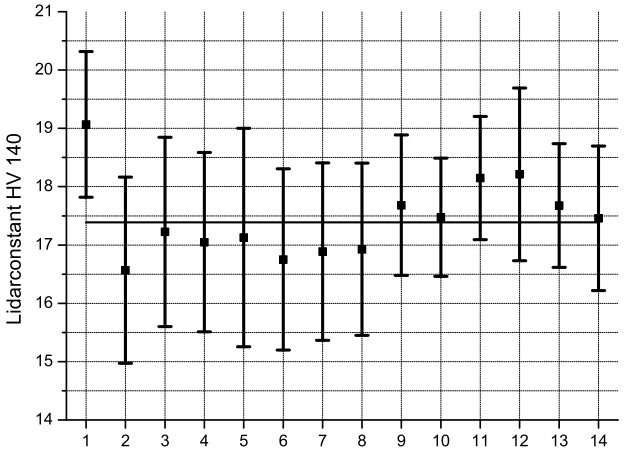

Fig. 4. Lidar constant C_{L}^{*} for $\Delta = 140$ as derived from 14 comparisons with AERONET optical depth.

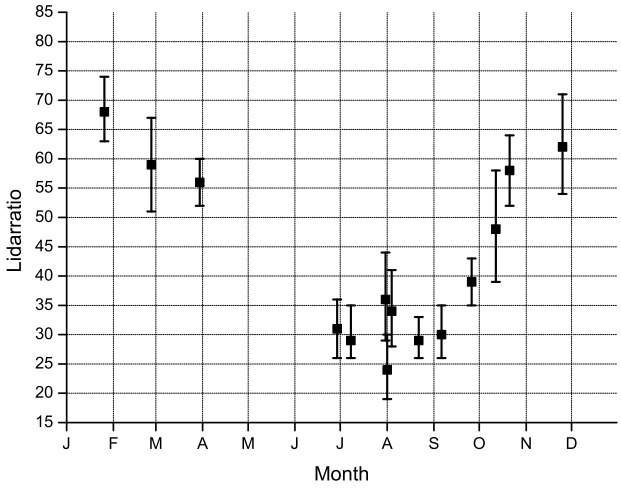

Fig. 5. Derived lidar ratios S_p at 1064 nm when τ_p from the ceilometer and AERONET agrees; shown are the 14 cases used for the absolute calibration of the ceilometer.

β_p-profiles makes more sense, e.g., when the top of the planetary boundary layer and the lower boundary of the clouds are well separated.

An example is shown in Fig. 1 when one of these changes occurs at 13:30 UTC. A conversion factor of $\eta_1 = 0.385$ is found here. It is important to emphasize that this change does not affect the Δ in the data files; only a special service code is set. As a consequence, it is not sufficient to consider Δ as the only criterion to determine the lidar constant; moreover, before the measurements are evaluated, it is required to check whether or not changes of the service code took place. The conversion factors should be determined individually for each change of the detector settings. This is in particular true when B exceeds 0.5 more than once during a day. Though this is tedious work, there are no fundamental problems associated with this procedure; one has only to be sure that the aerosol distribution is stable for a sufficient time period. For our ceilometer, we perform the determination of different conversion factors. However, it is not of general interest to publish these factors here.

At 01:00 UTC, these changes are reset and a new optimum Δ is selected. Depending on the previous Δ, a significant change of the system's sensitivity might be associated with this. This is obviously the case on 22 April 2010 as can be seen in Fig. 1. As a consequence, from 01:00 UTC, the lidar constant can be determined as described in the previous section.

5 Application

The potential of the calibration procedure to derive optical properties of aerosols is demonstrated for 22 April 2010. The result of normalizing the signals according to Eq. (10) at 06:57 UTC, 08:28 UTC, 18:24 UTC and 19:27 UTC, and η_1 at 13:30 UTC is shown in Fig. 6. As in Fig. 1, the range-corrected signal is plotted. It is clearly visible that all "steps" due to the changes of the sensitivity disappear. Thus, the "forward" Klett inversion using the lidar constant C_{L}^{*} (according to Eq. 1) can be used to determine aerosol backscatter profiles $\beta_p(z)$ at 1064 nm with a quite high temporal resolution. If we concentrate on the aerosol mixing layer, averages over 2 min are sufficient to retrieve "smooth" signals as will be shown later in more detail.

For illustrating quantitative retrievals of aerosol properties, a series of β_p-profiles (Fig. 7) and the diurnal cycle of τ_p (Fig. 8) are discussed. In Fig. 7 six profiles (every four hours starting from 02:00 UTC) are plotted. The maximum of the backscatter coefficient occurs in the morning in $z = 1.6$ km with $\beta_p = 0.0088\,\mathrm{km}^{-1}\,\mathrm{sr}^{-1}$ (not shown here). For the retrieval, we select a lidar ratio of $S_p = 43$ sr in accordance with the findings from the above mentioned 14 cases. The signals are averaged over 6 min and smoothed over two range bins. To reduce the complexity of the figure, we have not included error bars. The typical magnitude can, however, easily be estimated. The uncertainty of C_{L} is determined by the errors of C_{L}^{*} and η (see Sect. 4.2). A realistic uncertainty of S_p of ± 10 sr has virtually no influence on the systematic error of β_p; it is below 2 % in the boundary layer or even smaller if the optical depth is very low at 1064 nm. Thus, the accuracy of β_p is primarily determined by the error of the lidar constant.

To compare two independent data sets, we consider the aerosol optical depth τ_p. It can directly be derived from Cimel data and from integration of the α_p-profiles from the ceilometer. To make τ_p comparable, we extrapolate the optical depth from the wavelength of the Cimel measurements (1020 nm) to the ceilometer's wavelength (1064 nm) assuming a λ^{-1}-dependence of α_p. Note that the α_p-profiles from the ceilometer data are integrated up to 4 km only. Above

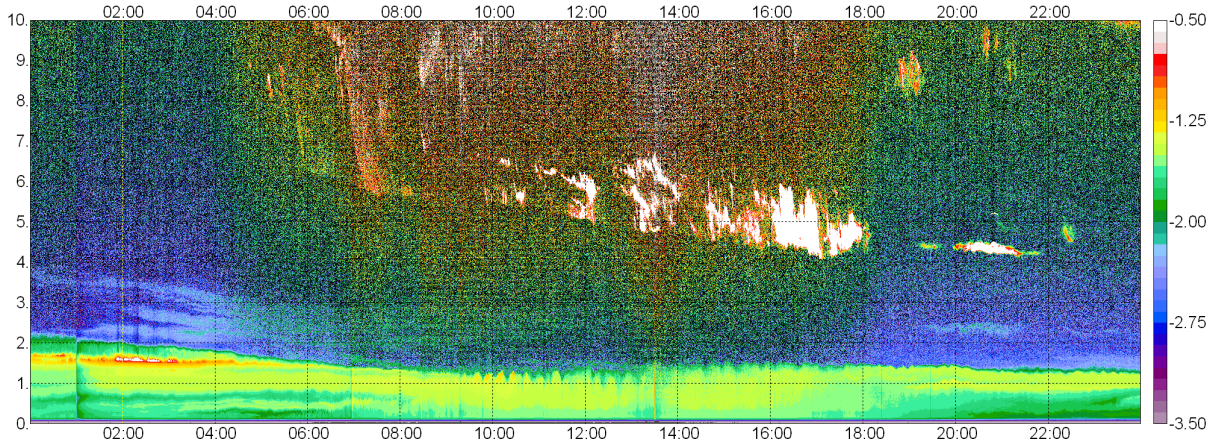

Fig. 6. Same as Fig. 1, but after the application of the conversions factors η and η_1 as described in the text.

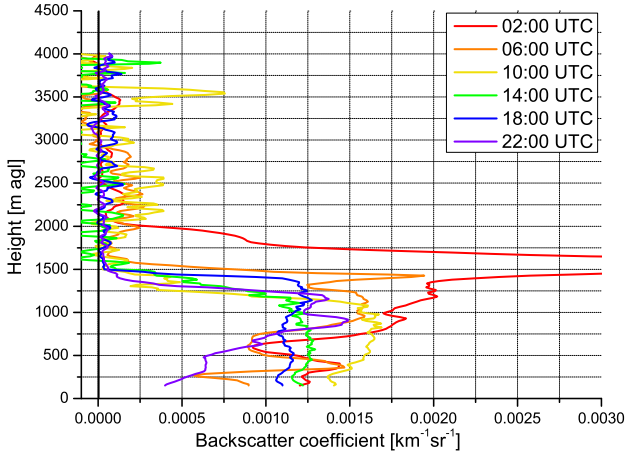

Fig. 7. Aerosol backscatter profiles β_p [in $\mathrm{km}^{-1}\,\mathrm{sr}^{-1}$] at 1064 nm from 0:00 UTC to 24:00 UTC, 22 April 2010, in intervals of four hours as indicated. Errors are omitted for the sake of clarity, but described in the text.

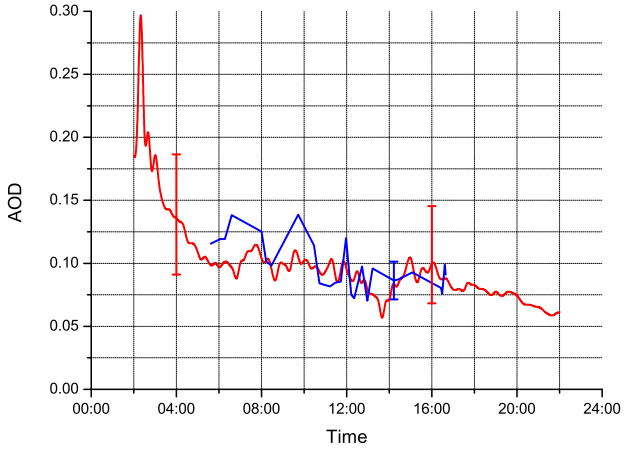

Fig. 8. Aerosol optical depth τ_p calculated by integrating α_p up to 4 km as derived from the ceilometer data (at 1064 nm, red curve) and the Cimel radiometer (extrapolated from 1020 nm to 1064 nm, blue curve) of 22 April 2010. Typical error bars are included to illustrate the accuracy of the retrieved τ_p.

4 km, the retrieval is too noisy for the integration; however, we do not expect a significant underestimate of τ_p as there are no indications of aerosol layers in the upper troposphere. Below z_{ovl}, the constant value $\alpha_p(z_{\mathrm{ovl}})$ is assumed for the extinction coefficient.

The diurnal cycle of 22 April 2010 is shown in Fig. 8. Sunrise and sunset are at 04:12 UTC and 18:14 UTC, respectively. From Fig. 8 two main conclusions can be drawn: first, the agreement between the two τ_p-retrievals is very good, though this day is not among the 14 cases used for the absolute calibration. Thus, the mean lidar ratio of 43 sr is obviously a good estimate in this case. However, it should be emphasized that the uncertainty of τ_p derived from the ceilometer is large. In contrast to the β_p-profiles, the uncertainty of the lidar ratio has a significant influence on α_p and consequently on τ_p. Assuming again an uncertainty of S_p of ± 10 sr (corresponding to 23 % relative error) and taking into account the uncertainty of C_{L} (4 %), the relative error of τ_p is calculated as 27 % if $\Delta = 140$. In cases with different instrument settings, the additional error of the (successive) application of η has to be considered resulting in an overall uncertainty of up to 30 %. For illustration, the calculated errors of τ_p for 04:00 UTC and 16:00 UTC are included in Fig. 8. The second conclusion is that the slight decrease of the aerosol optical depth during the daylight period as derived from Cimel measurements cannot be confirmed by the ceilometer measurements as the uncertainty is too large. The uncertainty is significantly reduced if the integrated backscatter (not shown here) is used as a measure of the overall temporal development. Then, the ceilometer retrievals demonstrate that the trend is not constant over

the full day. The peak shortly after 02:00 UTC and the large optical depth before 03:00 UTC are certainly due to hygroscopic aerosols in an environment of high relative humidity in 1.6 km (see Fig. 6). This example underlines that the extrapolation of optical depths from daytime to nighttime can be misleading; the assumption of a constant aerosol optical depth as well as the assumption of a constant change can be wrong.

It is worthwhile to compare vertically integrated aerosol optical depth (τ_p, Fig. 8) and the vertical aerosol distribution (β_p, Fig. 7). It can be seen that the aerosol distribution changes throughout the day: as already mentioned, a strong aerosol layer exists (maximum at 1.6 km) in the early morning. Over the course of the day, the height dependence of β_p changes significantly: at 06:00 UTC, different clearly separated layers are present; from 10:00 UTC till 18:00 UTC, the distribution is approximately height-independent, whereas at 22:00 UTC a strong increase of β_p from $z = 200$ m to $z = 900$ m is observed. The top of the mixing layer changes by approximately 300 m during the daylight period. The temporal variability of β_p is different in each altitude, and the magnitude of the changes is up to 50 % and more; in particular, close to the surface the variability is large. This is in clear contrast to the slow change of the aerosol optical depth during the same time period. This suggests (not unexpectedly) that no general relationship exists between τ_p and β_p at a certain height, e.g., at the surface. Ceilometer measurements can help to mitigate this problem: with the provision of β_p in the lowermost troposphere and the good temporal resolution, it is possible to link atmospheric and ground-based measurements more reliably than can be done with integrated properties.

An essential point of the benefit of aerosol remote sensing is the achievable temporal resolution of the profiles. This can be assessed individually by calculating the signal-to-noise ratio of any specific measurement (e.g., Wu et al., 2006). From our data, we conclude that for nighttime measurement averages over 2 min are fully sufficient to monitor the evolution of the boundary layer and the residual layer by means of β_p-profiles. To illustrate the daytime-capability of the ceilometer measurements, three different temporal resolutions of β_p-profiles are shown in Fig. 9. The additional profiles (dashed lines) illustrate the uncertainty range due to the unknown S_p and the error of C_L. As an example, we again consider 22 April 2010 and select the β_p-profile at 12:00 UTC, when the atmosphere above the boundary layer is apparently aerosol-free as suggested from Fig. 6. Averages over 30 s (i.e., the resolution of the raw data), 2 min and 20 min are shown for comparison. The signal-to-noise ratios are larger than 1 up to a height of 1600 m, 2100 m and 3000 m (not shown here) with typical values of 50, 100 and 300 in the boundary layer, respectively. Accordingly, the vertical structure of the boundary layer below $z = 1400$ m can be resolved in all three cases. However, above this layer, noise prevents the detection of any aerosol layer in the case of 30 s and

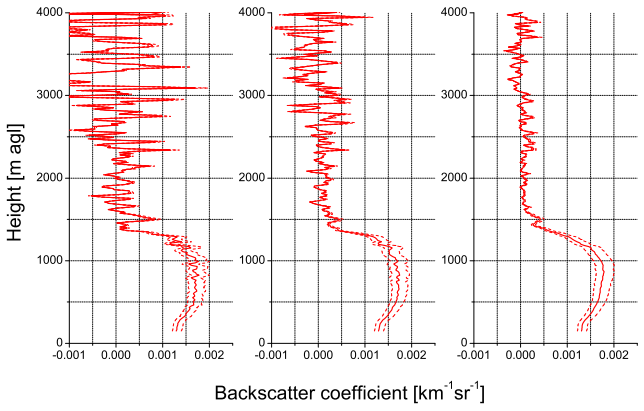

Fig. 9. Profiles of aerosol backscatter coefficients $\beta_p(z)$ [in $\mathrm{km}^{-1}\,\mathrm{sr}^{-1}$] at 1064 nm (22 April 2010, 12:00 UTC) averaged over 30 s, 2 min and 20 min (from left to right). The dashed lines illustrate the range of possible solutions due to the error of C_L and the uncertainty of S_p.

2-min averages. If longer time averages are considered (e.g., 20 min; see right panel), the presence of elevated aerosol layers can be excluded.

The potential of the ceilometer to monitor elevated aerosol layers is demonstrated by another example (21 August 2011). In Fig. 10 we show a sequence of eight 2-min averages in intervals of 50 min between 02:00 UTC and 07:50 UTC. The signals are smoothed over 30 m along the line of sight. It can be seen that small-scale variations are resolved. For instance, the evolution of the pronounced aerosol layer between 3 km and 4 km can be clearly monitored, as its backscatter coefficient is as large as β_p in the boundary layer. Though the retrieved profiles become more noisy, the existence and the extent of this optically thick elevated layer can be documented even after sunrise (04:16 UTC). The errors of β_p are the same as described before and thus are omitted in the figure.

Finally, we want to present an example of a quantitative analysis of ceilometer data covering a full month. We calculate the aerosol optical depth at 1064 nm on a daily basis for March 2011, applying a constant lidar ratio of $S_p = 43$ sr for all cases. In Fig. 11 nighttime and daytime values are plotted separately. Nighttime values are calculated from 2-min averages at 02:00 UTC, whereas the corresponding measurements at 14:00 UTC are selected to represent daytime values; only in cases of low clouds, deviations of up to one hour are accepted. Gaps in the time series are due to high and persistent cloudiness or precipitation. The optical depth is determined from ground (including the extrapolation as described above) up to an altitude of typically 4 km or 5 km. The main criterion for the choice of the upper level is that elevated aerosol layers – if present – are included; then it is possible to compare τ_p derived from ceilometer measurements with independent data sets. From Fig. 11 a large variability of τ_p,

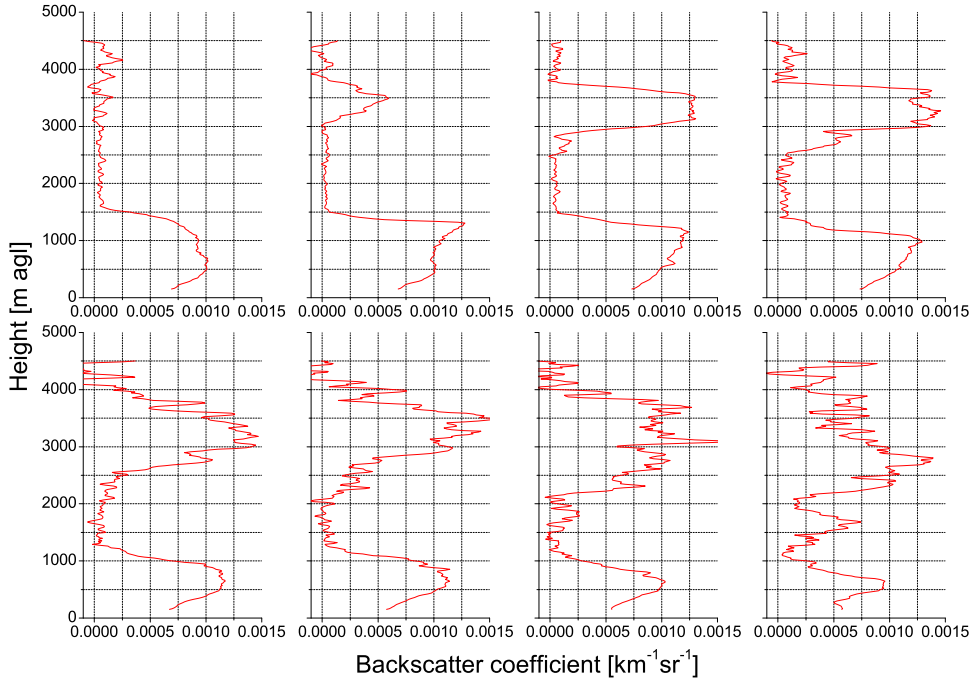

Fig. 10. Profiles of aerosol backscatter coefficients $\beta_p(z)$ [in $\mathrm{km}^{-1}\,\mathrm{sr}^{-1}$] at 1064 nm from 02:00 UTC till 07:50 UTC in intervals of 50 min (21 August 2011). Each profile is averaged over 2 min.

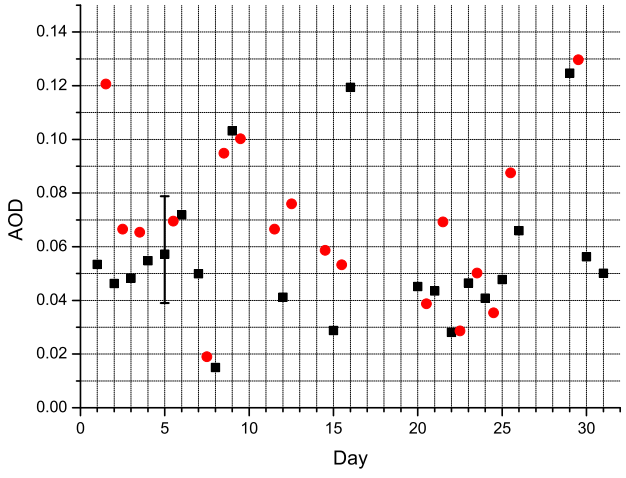

Fig. 11. Aerosol optical depth at 1064 nm as derived from the inversion of the ceilometer data of March 2011, separately for nighttime (red dots) and daytime (black squares). As an example, we include the uncertainty range of the nighttime measurement of 5 March 2011.

from day to day but also from night to the subsequent day or vice versa, is obvious.

For March 2011, we find a monthly mean optical depth at 1064 nm of 0.068 and 0.056 for daytime and nighttime, respectively. Assuming an Ångström exponent between 1 and 1.5 leads to an optical depth at 532 nm of $0.12 < \tau_p <$ 0.18, which is a plausible value for Munich. However, the error of τ_p is on the order of 25–30 % as discussed before; for illustration it is sufficient to include one typical example (5 March 2011). This large uncertainty makes it impossible to resolve the difference between successive daytime and nighttime optical depths. Only if we assume that the lidar ratio does not change from day to night, the difference can be determined. Then, it is 0.024 on average but it can be as large as 0.08. Only in 6 out of 15 cases, the difference is below 20 %.

6 Conclusions

The assessment of the performance of ceilometers for aerosol remote sensing is urgently needed in view of the rapidly increasing number of such "simple backscatter lidars". As a consequence of the low laser pulse energy, calibration of the signals is challenging. In this paper, we elaborate a method for the absolute calibration of the Jenoptik ceilometer CHM15kx. The advantage of this approach is obvious: whereas the calibration relies only on measurements under favorable conditions resulting in a high accuracy, the retrieval of profiles of β_p is possible under virtually any meteorological condition – daytime and nighttime – with a temporal resolution of a few minutes. This offers a wide range of applications: it is possible to monitor profiles of the particle backscatter coefficient, to study correlations between integral quantities (integrated backscatter, optical depth) with

the aerosol backscatter coefficient close to the surface, or to investigate the full diurnal cycle of the aerosol optical depth. Moreover, if a network of ceilometers is available, the horizontal distribution of aerosols can be assessed. A very important advantage of our approach is that it can easily be automated to evaluate large data sets, e.g., to establish an aerosol climatology. The main drawback of ceilometer data is the low signal-to-noise ratio in the free troposphere compared to more powerful lidar systems. As a conclusion, elevated aerosol layers cannot be resolved if their optical depth is very low or if the optical depth of the boundary layer is very large. The low signal-to-noise ratio does not, however, prevent the inversion of β_p in the mixing layer, because the data evaluation starts – in contrast to the standard Klett retrieval – close to the surface ("forward integration"). In this altitude range, typical signal-to-noise ratios on the order of 100 or more are found, even if averages of not more than 2 min are considered.

The accuracy of the aerosol retrieval depends on the accuracy of the lidar constant of the ceilometer. According to our study, the relative error of (reference) lidar constant C_{L}^{*} is as low as 4 %. Additional small errors must be considered in case of the Jenoptik CHM15kx because of the changing APD-settings. In summary, we find that the relative errors of β_p profiles are less than 8 %. Large errors are introduced when an estimate of the lidar ratio is required, e.g., for the retrieval of extinction coefficients. This is, however, an inherent problem of any system – ceilometer or lidar – that is based on the backscatter lidar technology. Note that the lidar ratio at 1064 nm cannot be determined from Raman lidars, so that one has to rely on model calculations, on (rare) comparisons with co-located and coincident sun photometer measurements, or independent measurements (e.g., high spectral resolution lidar). As a consequence, optical properties that are related to the extinction coefficient must be treated with care. The same is true, if surface values are extrapolated from integral values, e.g., from aerosol optical depth or integrated backscatter.

In case of the CHM15kx, the determination of the lidar constant is tedious work as the sensitivity of the system changes with the solar background. However, due to the very low overlap, data from the CHM15kx can provide a limited but very useful set of aerosol information. For ceilometers with a "constant" lidar constant, absolute calibration in principle should be easier. This is the case for the Jenoptik CHM15k – a recent upgrade ("Nimbus") providing a calibration pulse for each signal might further facilitate the absolute calibration. On the other hand, absolute calibration is significantly complicated and subject to potentially large errors if the ceilometer has a large range of complete overlap (e.g., 500 m or even more). Then, a reliable overlap correction is indispensable for calibration.

Acknowledgements. The authors are grateful to Steffen Frey and Holger Wille (Jenoptik) for technical information about the CHM15kx.

Edited by: V. Amiridis

References

Ansmann, A., Wagner, F., Althausen, D., Müller, D., Herber, A., and Wandinger, U.: European pollution outbreaks during ACE 2: Lofted aerosol plumes observed with Raman lidar at the Portuguese coast, J. Geophys. Res., 106, 20725–20733, 2001.

Böckmann, C.: Hybrid regularization method for the ill-posed inversion of multiwavelength lidar data in the retrieval of aerosol size distributions, Appl. Optics, 40, 1329–1342, 2001.

Bösenberg, J., Matthias, V., Amodeo, A., Amoiridis, V., Ansmann, A., Baldasano, J. M., Balin, I., Balis, D., Böckmann, C., Boselli, A., Carlsson, G., Chaikovsky, A., Chourdakis, G., Comeron, A., De Tomasi, F., Eixmann, R., Freudenthaler, V., Giehl, H., Grigorov, I., Hagard, A., Iarlori, M., Kirsche, A., Kolarov, G., Komguem, L., Kreipl, S., Kumpf, W., Larcheveque, G., Linné, H., Matthey, R., Mattis, I., Mekler, A., Mironova, I., Mitev, V., Mona, L., Müller, D., Music, S., Nickovic, S., Pandolfi, M., Papayannis, A., Pappalardo, G., Pelon, J., Perez, C., Perrone, R. M., Persson, R., Resendes, D. P., Rizi, V., Rocadenbosch, F., Rodrigues, J. A., Sauvage, L., Schneidenbach, L., Schumacher, R., Shcherbakov, V., Simeonov, V., Sobolewski, P. , Spinelli, N., Stachlewska, I., Stoyanov, D., Trickl, T., Tsaknakis, G., Vaughan, G., Wandinger, U., Wang, X., Wiegner, M., Zavrtanik, M., and Zerefos, C.: EARLINET: A European Aerosol Research Lidar Network to Establish an Aerosol Climatology, MPI-Report 348, Max-Planck-Institut für Meteorologie, Hamburg, Germany, 192 pp., ISSN 0937–1060, 2003.

Emeis, S., Münkel, C., Vogt, S., Müller, W., and Schäfer, K.: Atmospheric boundary-layer structure from simultaneous SODAR, RASS, and ceilometer measurements, Atmos. Environ., 38, 273–286, 2004.

Fernald, F. G.: Analysis of atmospheric lidar observations: some comments, Appl. Optics, 23, 652–653, 1984.

Fernald, F. G., Herman, B. M., and Reagan, J. A.: Determination of aerosol height distributions by lidar, J. Appl. Meteorol. 11, 482–489, 1972.

Flamant, C., Pelon, J., Chazette, P., Trouillet, V., Quinn, P. K., Frouin, R., Bruneau, D., Leon, F., Bates, T. S., Johnson, J., and Livingston, J.: Airborne lidar measurements of aerosol spatial distribution and optical properties over the Atlantic Ocean during a European pollution outbreak of ACE-2, Tellus B, 52, 662–677, doi:10.1034/j.1600-0889.2000.00083.x, 2000.

Gasteiger, J., Groß, S., Freudenthaler, V., and Wiegner, M.: Volcanic ash from Iceland over Munich: mass concentration retrieved from ground-based remote sensing measurements, Atmos. Chem. Phys., 11, 2209–2223, doi:10.5194/acp-11-2209-2011, 2011.

Groß, S., Tesche, M., Freudenthaler, V., Toledano, C., Wiegner, M., Ansmann, A., Althausen, D., and Seefeldner, M.: Characterization of Saharan dust, marine aerosols and mixtures of biomass burning aerosols and dust by means of multi-wavelength depolarization- and Raman-measurements during SAMUM-2,

Tellus B, 63, 706–724, doi:10.1111/j.1600-0889.2011.00556.x, 2011.

Haeffelin, M., Angelini, F., Morille, Y., Martucci, G., Frey, S., Gobbi, G. P., Lolli, S., O'Dowd, C. D., Sauvage, L., Xueref-Rémy, I., Wastine, B., and Feist, D. G.: Evaluation of Mixing-Height Retrievals from Automatic Profiling Lidars and Ceilometers in View of Future Integrated Networks in Europe, Bound.-Lay. Meteorol., 143, 49–75, doi:10.1007/s10546-011-9643-z, 2011.

Heese, B. and Wiegner, M.: Vertical aerosol profiles from Raman polarization lidar observations during the dry season AMMA field campaign, J. Geophys. Res., 113, D00C11, doi:10.1029/2007JD009487, 2008.

Heese, B., Flentje, H., Althausen, D., Ansmann, A., and Frey, S.: Ceilometer lidar comparison: backscatter coefficient retrieval and signal-to-noise ratio determination, Atmos. Meas. Tech., 3, 1763–1770, doi:10.5194/amt-3-1763-2010, 2010.

Holben, B. N., Eck, T. I., Slutsker, I., Tanré, D., Buis, J. P., Setzer, A., Vermote, E., Reagan, J. A., Kaufman, Y. J., Nakajima, T., Lavenu, F., Jankowiak, I., and Smirnov, A.: AERONET – A Federated Instrument Network and Data Archive for Aerosol Characterization, Remote Sens. Environ., 66, 1–16, 1998.

Klett, J. D.: Stable analytical inversion solution for processing lidar returns, Appl. Optics, 20, 211–220, 1981.

Kolgotin, A. and Müller, D.: Theory of inversion with two-dimensional regularization: profiles of microphysical particle properties derived from multiwavelength lidar measurements, Appl. Optics, 47, 4472–4490, 2008.

Martucci, G., Milroy, C., and O'Dowd, C. D.: Detection of Cloud-Base Height Using Jenoptik CHM15K and Vaisala CL31 Ceilometers, J. Atmos. Ocean. Tech., 27, 305–318, 2010.

McKendry, I. G., van der Kamp, D., Strawbridge, K. B., Christen, A., and Crawford, B.: Simultaneous observations of boundary-layer aerosol layers with CL31 ceilometer and 1064/532 nm lidar, Atmos. Environ., 43, 5847–5852, 2009.

Müller, D., Wagner, F., Althausen, D., Wandinger, U., and Ansmann, A.: Physical properties of an Indian aerosol plume derived from 6-wavelength lidar observations on 25 March 1999 of the Indian Ocean Experiment, Geophys. Res. Lett., 27, 1403–1406, 2000.

Münkel, C., Eresmaa, N., Räsänen, J., and Karppinen, A.: Retrieval of mixing height and dust concentration with lidar ceilometer, Bound.-Lay. Meteorol., 124, 117–128, 2007.

Shimizu, A., Sugimoto, N., Matsui, I., Arao, K., Uno, I., Murayama, T., Kagawa, N., Aoki, K., Uchiyama, A., and Yamazaki, A.: Continuous observations of Asian dust and other aerosols by polarization lidars in China and Japan during ACE-Asia, J. Geophys. Res., 109, D19S17, doi:10.1029/2002JD003253, 2004.

Sicard, M., Rocadenbosch, F., Hénon, A., Pérez, C., Rodríguez, A., Muñoz, C., García Vizcaíno, D., Comerón, A., and Baldasano, J. M.: Evidence of discrepancies between columnar averaged lidar ratios measured by sun photometer and lidar by means of a Raman lidar in Barcelona, Proc. 23rd International Laser Radar Conference, 24–28 July 2006, Nara, Japan, 437–440, 2006.

Stachlewska, I. S., Markowicz, K. M., and Piadlowski, M.: On forward Klett's inversion of ceilometer signals, Proc. 25th ILRC International Laser Radar Conference, 5–9 July 2010, St. Petersburg, Russia, 1154–1157, 2010.

Takamura, T., Sasano, Y., and Hayasaka, T.: Tropospheric aerosol optical properties derived from lidar, sun photometer, and optical particle counter measurements, Appl. Optics, 33, 7132–7140, 1994.

Tesche, M., Groß, S., Ansmann, A., Müller, D., Althausen, D., Freudenthaler, V., and Esselborn, M.: Profiling of Saharan dust and biomass-burning smoke with multiwavelength polarization Raman lidar at Cape Verde, Tellus B, 63, 649–676, doi:10.1111/j.1600-0889.2011.00548.x, 2011.

Wiegner, M.: Potential of ceilometers for aerosol remote sensing: a preliminary assessment, Proc. 25th International Laser Radar Conference, 5–9 July 2010, St. Petersburg, Russia, 914–917, 2010.

Wiegner, M., Emeis, S., Freudenthaler, V., Heese, B., Junkermann, W., Münkel, C., Schäfer, K., Seefeldner, M., and Vogt, S.: Mixing layer height over Munich, Germany: Variability and comparisons of different methodologies, J. Geophys. Res., 111, D13201, doi:10.1029/2005JD006593, 2006.

Wu, S., Liu, Z., and Liu, B.: Enhancement of lidar backscatters signal-to-noise ratio using empirical mode decomposition method, Opt. Comm., 267, 137–144, doi:10.1016/j.optcom.2006.05.069, 2006.